

ARTICLE

Structure and electrochemical performance of LiFePO₄ modified with mononuclear and binuclear phthalocyanines as cathode materials

Feifei Xu, Ruiqiong Wang, Ronglan Zhang,^{a)} and Jianshe Zhao^{b)}

Key Laboratory of Synthetic and Natural Functional Molecule Chemistry of Ministry of Education, College of Chemistry and Materials Science, Northwest University, Xi'an, Shaanxi 710069, People's Republic of China

(Received 4 November 2016; accepted 27 December 2016)

Two series of lithium iron phosphate (LiFePO₄) nanocomposites are prepared by a solvothermal method coupled with high temperature calcination using mononuclear and binuclear metal hexaaminophthalocyanines as modulatory additives, respectively. Physical and electrochemical performances of the composites as cathode materials of lithium-ion batteries are characterized by inductively coupled plasma (ICP), X-ray diffraction (XRD), infrared (IR), scanning electron microscopy (SEM), transmission electron microscopy (TEM), and electrochemical techniques. The results indicate that the as-synthesized samples modified with binuclear metal phthalocyanines can improve electrochemical properties of LiFePO₄ (LFP) for lithium-ion batteries. The composite using binuclear manganese hexaaminophthalocyanine as additive can achieve the highest initial specific discharge capacity of 152.3 mAh/g at 0.1 C, higher than that of ones modified with the corresponding mononuclear phthalocyanine 143.0 mAh/g. Furthermore, the most excellent product exhibits a pretty good capacity retention of 93.0% after 50 cycles at 0.1 C, cycling stability, and low charge transfer resistance of 58.7 Ω.

I. INTRODUCTION

Lithium-ion batteries (LIBs) have taken dominating position in powering and portable electronic devices in recent years, which is due to their obvious advantages such as high power and energy density, rechargeable ability, long cycling life, great stability, and safety.^{1,2} Compared with a variety of cathode materials including layered LiCoO₂ and spinel LiMn₂O₄, ordered olivine-structured LiFePO₄ has attracted extensive attention owing to its high theoretical capacity of 170 mAh/g, acceptable voltage platform of 3.4 V (versus Li⁺/Li), nontoxicity, low cost, good safety, thermal stability, as well as environmental benignity.^{3,4} The phosphorous atoms occupy tetrahedral sites, while the iron and lithium atoms occupy octahedral sites. The FeO₆ octahedra are linked through common corners in the *bc*-plane, and the LiO₆ octahedra form edge-sharing chains along the *b*-axis. One FeO₆ octahedron has common edges with two LiO₆ octahedra and a PO₄ tetrahedron. PO₄ groups share one edge with an FeO₆ octahedron and two edges with LiO₆ octahedra.⁵ However, the intrinsic drawbacks, low electronic conductivity and sluggish lithium-ion diffusion,

create obstacles in the widespread application of the material in LIBs.⁶

Fortunately, the barrier can be hurdled through diversified modifications of LiFePO₄. Among numerous endeavors, methods containing carbon coating, foreign elements doping, morphological controlling, and synthesis of nanoparticles can improve the electrochemical performance of the composites efficiently.^{7–11} Nevertheless, a single approach is not enough, excessive carbon coated on the surface of particles would decline the overall energy density of the material, and superabundant metal doped in the composite would bring about defects overmuch, thus doing harm to the cycling stability of the battery.¹² The combination of carbon coating and metal doping has been certified to be an effective way to improve the capabilities of the materials.¹³ To provide the two factors simultaneously, we employ mononuclear metal phthalocyanines (MPcs) as additives during the solvothermal process in our previous work,^{14,15} which fulfills the requirement more easily. MPcs with 18π electrons conjugated system possess great properties such as thermal stability, oxidation-reduction activity, nontoxicity, and low cost, which enable them to be excellent modifiers and cathode replacing materials of LIBs.¹⁶ Furthermore, carbon coating derived from the pyrolysis of organics could efficiently increase the electrical conductivity, at the same time, *in situ* decoration of carbon coating can also limit the crystal growth and restrain from agglomeration.⁶

Contributing Editor: Chongmin Wang
Address all correspondence to these authors.
^{a)}e-mail: zhangrl@nwu.edu.cn
^{b)}e-mail: jszhao@nwu.edu.cn
DOI: 10.1557/jmr.2017.16

In previous works,^{14,15} LiFe_{1-x}M_xPO₄/C ($x \approx 0.0040$) composites were synthesized with highly improved electrochemical performances. For further studying the influence of MPcs on LiFePO₄, mononuclear metal tetraaminophthalocyanines and binuclear metal hexaaminophthalocyanines [MPcTa and M₂Pc₂Ha, M = Mn(II), Co(II), Ni(II), Cu(II), Zn(II)] were adopted as additives to decorate LiFePO₄ in this paper. Structures and morphologies were investigated by using normal characterization such as X-ray diffraction (XRD), scanning electron microscopy (SEM), and transmission electron microscopy (TEM) measurements. In addition, the relevant electrochemical performance was also studied.

II. EXPERIMENTAL

A. Composite synthesis

All the chemicals were analytical grade and used without further purification.

MPcTa [M = Mn(II), Co(II), Ni(II), Cu(II), Zn(II)] was prepared according to the reported method.¹⁷ M₂Pc₂Ha [M = Mn(II), Co(II), Ni(II), Cu(II), Zn(II)] was synthesized on the basis of the reported method¹⁸ by changing the carboxyl of the raw material into an amino group. The modified LiFe_{1-x}M_xPO₄/C was synthesized by using a modified solvothermal process. The precursor 0.0200 mol LiOH·H₂O (AR, Aladdin, Shanghai, China) was dissolved in a mixed solvent (EG:DMF = 3:1, v/v) to form a homogeneous solution. 2.3 mL H₃PO₄ (85%, AR), 0.0067 mol FeSO₄·7H₂O (AR, Aladdin) and 0.200 mmol^{19,20} MPcTa or M₂Pc₂Ha were added slowly to the solution (controlled a weight ratio of Li:Fe:P = 3:1:1) with magnetic stirring for 0.5 h at room temperature, until a green mixture was formed, and the concentration of Li⁺ was maintained at 0.5 mol/L. The solution prepared above was transferred to a 60 mL Teflon-lined stainless steel autoclave for a solvothermal procedure at 180 °C for 18 h. After that, the reacted mixture was cooled down naturally to ambient temperature, filtered, and washed thoroughly with deionized water until its pH reached 7. The resulting solvothermal precursors were collected and dried at 80 °C for 24 h. The powder was heat-treated at 700 °C for 5 h under N₂ atmosphere to form LiFe_{1-x}M_xPO₄/C [$x \approx 0.0040$; M = Mn(II), Co(II), Ni(II), Cu(II), Zn(II)] composites. The pure LiFePO₄ (LFP) was prepared under the same conditions without any MPcTa or M₂Pc₂Ha.

The as-synthesized composites using MPcTa [M = Mn(II), Co(II), Ni(II), Cu(II), Zn(II)] as additives are denoted as a1, a2, a3, a4, and a5, and composites using M₂Pc₂Ha [M = Mn(II), Co(II), Ni(II), Cu(II), Zn(II)] as additives are denoted as b1, b2, b3, b4, and b5, respectively.

B. Materials characterization

Contents of metal and carbon in samples were detected on inductively coupled plasma atomic emission

spectrometry (ICP-AES; 2100DV, Perkin Elmer, Norwalk, California) and C, H, N Analyzer model 1106 Carlo Erba Strumentazione (Carlo Erba Strumentazione, Milan, Italy). XRD (D8 Advance, Bruker Inc., Karlsruhe, Germany) was used in a scanning range of 10–80° (2θ) using Cu K_α radiation; the X-ray tube voltage and current were set at 40 kV and 40 mA to characterize the crystallinity of each composite. Infrared (IR) spectra were collected on a Bruker VECTOR 22 analyzer (Bruker Inc.) by using KBr pellets in the infrared region of 400–4000 cm⁻¹. Morphologies were studied using SEM (JSM-6390A, JEOL Ltd., Tokyo, Japan) and TEM (Tecnai G2 F20 S-TWIN, FEI Company, Eindhoven, The Netherlands). Further information about the modification was achieved on X-ray photoelectron spectroscopy (XPS; HI-540, PE Co., Palo Alto, California).

C. Electrochemical test

The active materials (a1–a5, b1–b5, and pure LFP, respectively), acetylene black, and poly vinyl difluoride (PVDF) were mixed in the weight ratio of 75:15:10 in N-methyl pyrrolidone (NMP) to fabricate composite cathodes. The cathodes were assembled into CR2016 coin-type cells in the condition of Ar atmosphere. Lithium metal plate, Celgard 2400 membrane, and 1 M LiPF₆ in 1:1 ethylene carbonate (EC)/diethyl carbonate (DEC) (LP30, Merck) were adopted as an anode, a separator, and an electrolyte, respectively. Electrochemical properties of the assembled batteries were studied by using a charge/discharge instrument (Model Land CT2001A, Wuhan Jinnuo Electronics Co. Ltd., Wuhan, China) and electrochemical workstation (RST 5000, Zhengzhou Shiruisi Technology Co. Ltd., Shiruisi, China). All the tests were implemented at ambient temperature.

III. RESULTS AND DISCUSSIONS

A. Elemental composition, IR spectra, and structure and morphological characterization of the composite materials

ICP-AES and elemental analysis are used to detect the elemental compositions of the composite materials, which are reported in Table I. It can be confirmed that the doped metals and carbon derived from MPcTa or M₂Pc₂Ha are introduced into the composites, and a general formula is obtained as LiFe_{1-x}M_xPO₄/C [$x \approx 0.0040$; M = Mn(II), Co(II), Ni(II), Cu(II), Zn(II)].

The XRD patterns of a1–a5 and b1–b5 are shown in Fig. 1. All the diffraction peaks of the samples are corresponding with the PDF#83-2092 standard card,^{21,22} and there are no obvious impurity peaks, which indicate that the composites have well-crystallized orthorhombic olivine structures with a space group of *Pnma*. The

relative intensity of the diffraction peaks is slightly different from each plane, but all diffraction peaks (111) of samples are higher than that at (211) [Fig. 1(a)]. It is described that Li and Fe atoms of composites do not occur shuffling. The diffraction peaks (111) of the b1 and b3 are higher than their diffraction peaks (211); in contrast, the diffraction peaks (111) of b2, b4, and b5 are slightly weaker than or equal to the diffraction peaks (211) [Fig. 1(b)]. The results demonstrate that the latter three samples have a certain degree of distortions. Furthermore, no diffraction peak related to carbon in the XRD patterns indicates that the carbon content in the synthesized materials is low, or in which the carbon existed in the form of amorphous carbon. Thus these can affect the LFP structure of the samples. The diffraction peaks' intensity ratio of all samples $I(020)/I(200)$ is larger than that of the standard card, which could be attributed to the extraction and insertion of Li^+ in the material. It is beneficial to the electrochemical kinetics of samples as cathode electrode material for LIBs.²³ It is worth noting that the 2θ of diffraction peak positions of a1–a5 and b1–b5 composites slightly increase compared with the pure LFP, on account of the lattice distortion induced by the doped metals in the formation of a LFP structure. The

lattice parameters and unit cell volume of the all composites are obtained by the calculation method (Table II). As can be seen, the parameters of the samples are in the vicinity of the stander parameters, which indicates that the doped metals coming from the pyrolysis of MPcTa or M₂Pc₂Ha do not change the crystal structures of these samples, and suggesting a better stability and cycle performance of the materials.

The chemical structures of all composites are investigated by IR spectroscopy (Fig. 2). The absorption peaks in a region of 1063–1097 cm⁻¹ are due to the PO₄³⁻ groups of asymmetrical stretching vibration. In the region 972–980 cm⁻¹, the peaks are corresponding to the symmetrical stretching vibration P–O. Accordingly, at around 630 cm⁻¹ and 550 cm⁻¹, peaks are assigned to the asymmetrical bending vibration and the symmetrical bending vibration of PO₄³⁻, respectively. In addition, the bands at 3430 cm⁻¹ are associated with the stretching mode of –OH in H₂O. The absorption peaks existed in around 500 and 470 cm⁻¹ should be responsible for the transfer of Li⁺. And absorption peaks of C–O are found at about 1138 cm⁻¹; the results indicate a little organic carbon on the surface of each sample, which can enhance the contact among the particles of the samples and further increase the conductivity of the materials.

The SEM images of the particles are displayed in Fig. 3. From the SEM images, the morphologies of samples a3, a4, and a5 with respect to a1 and a2 form a more serious aggregation of particles, especially a4 presents a more serious bulk shape. Compared with sample a2, a1 shows relatively uniform spherical particles.²⁴⁻²⁷ The images of samples b4 and b5 show heavily aggregated block shape and lamellar morphology; the images of samples b1, b2, and b3 show more dispersed spherical particles. Compared with samples b2 and b3, sample b1 shows relatively uniform spherical small particles. It should be noticed that the morphologies of these samples vary significantly. This phenomenon is mainly due to the action of different metals derived from MPcTa and M₂Pc₂Ha as modified additives on LFP.

Sample	Percentage content (wt%)		Formula
	Metal	Carbon	
a1	Mn: 0.1418	3.1	$\text{LiFe}_{0.9958}\text{Mn}_{0.0042}\text{PO}_4/\text{C}$
a2	Co: 0.1378	2.9	$\text{LiFe}_{0.9962}\text{Co}_{0.0038}\text{PO}_4/\text{C}$
a3	Ni: 0.1482	2.8	$\text{LiFe}_{0.9959}\text{Ni}_{0.0041}\text{PO}_4/\text{C}$
a4	Cu: 0.1524	3.0	$\text{LiFe}_{0.9961}\text{Cu}_{0.0039}\text{PO}_4/\text{C}$
a5	Zn: 0.1491	2.8	$\text{LiFe}_{0.9963}\text{Zn}_{0.0037}\text{PO}_4/\text{C}$
b1	Mn: 0.1517	3.2	$\text{LiFe}_{0.9955}\text{Mn}_{0.0045}\text{PO}_4/\text{C}$
b2	Co: 0.1559	2.9	$\text{LiFe}_{0.9957}\text{Co}_{0.0043}\text{PO}_4/\text{C}$
b3	Ni: 0.1406	3.1	$\text{LiFe}_{0.9961}\text{Ni}_{0.0039}\text{PO}_4/\text{C}$
b4	Cu: 0.1563	3.0	$\text{LiFe}_{0.9960}\text{Cu}_{0.0040}\text{PO}_4/\text{C}$
b5	Zn: 0.1691	2.9	$\text{LiFe}_{0.9958}\text{Zn}_{0.0042}\text{PO}_4/\text{C}$

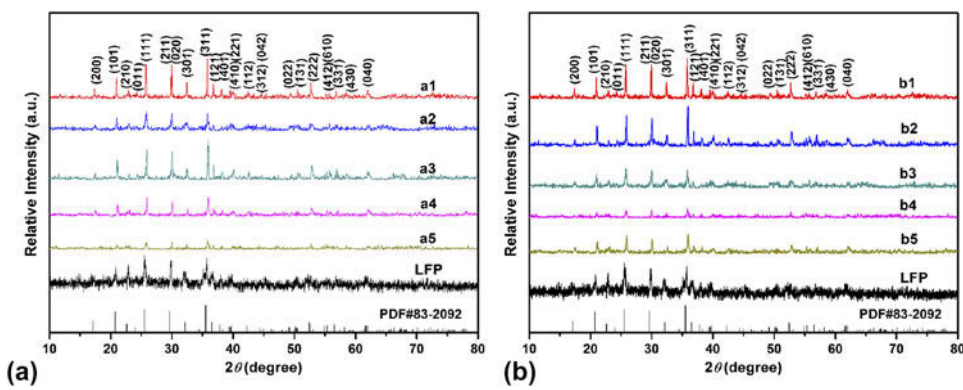


FIG. 1. XRD patterns of (a) a1, a2, a3, a4, and a5 and (b) b1, b2, b3, b4, and b5.

In theory, the uniform distribution without coalescing or less coalesced will be more conducive to improving the electrical properties of the material. Among all the samples, the morphologies of a1 and b1 in the same type are relatively better. And the diffusion path of Li⁺ can be efficiently shortened due to the small particle size in a1 and b1. The results indicate that the more excellent electrochemical performance should be provided by a1 and b1, which is confirmed by the electrical performance test later. High resolution transmission electron microscopy (HRTEM) is performed for further investigation of the carbon coated on LFP particles. The images of a1 and b1 show a conductive carbon layer on the edge of the materials. It indicates that the pyrolysis of MPcTa and M₂Pc₂Ha is carried out on an inert atmosphere by high temperature calcination, which generates the amorphous carbon coated on the LiFePO₄ particles to improve the electrochemical properties of the materials.

B. Electrochemical property

Two series of composite materials as cathode materials are assembled into a half cell configuration, then the related electrical properties are tested and analyzed. The initial charge/discharge specific curves at 0.1 C are showed in Fig. 4, and the corresponding data are listed in

TABLE II. Lattice parameters and unit cell volume of composite materials.

Sample	<i>a</i> (Å)	<i>b</i> (Å)	<i>c</i> (Å)	<i>V</i> (Å ³)
a1	10.33825	6.01129	4.69187	291.58
a2	10.33555	6.01122	4.69532	291.72
a3	10.33908	6.00366	4.69674	291.54
a4	10.33370	6.00740	4.69558	291.50
a5	10.33808	6.00920	4.69467	291.65
b1	10.32622	6.01591	4.69277	291.52
b2	10.33790	6.00965	4.69133	291.46
b3	10.32089	5.98386	4.67801	288.91
b4	10.32878	6.01723	4.69675	291.90
b5	10.33153	6.01240	4.68303	290.90
PDF#83-2092	10.334	6.01	4.693	291.47

Table III. The charge and discharge process of the battery, the cathode transformation between phase orthorhombic of LiFePO₄, and the hexagonal system of FePO₄ because LiFePO₄ and FePO₄ coexist to form a solid solution below 200 °C, there is no obvious two phase turning point in the process of charging/discharging. Therefore, all the samples show a longer and more flat charge/discharge platforms. And charge/discharge platforms of the samples at around 3.4–3.5 V, which could be the main characteristic of the two-phase reaction based on the redox couple of Fe³⁺/Fe²⁺ during the process of extraction and insertion of Li⁺.²⁸ The charging and discharging platforms of composites are longer than that of pure LFP, suggesting that the electrochemical activity and kinetic properties of the composites are better than the pure LFP. The composites of a1–a5 can deliver higher initial specific discharge capacities of 143.0, 132.7, 125.1, 110.9, and 123.6 mAh/g and b1–b5 of 152.3, 149.2, 147.7, 132.9, and 116.8 mAh/g at 0.1 C, respectively, which are all improved compared with pure LFP (109.2 mAh/g) under the same conditions, especially the a1 and b1 can increase by 31.0% and 39.5%, respectively (Fig. 4, Table III). Results shown in Fig. 4 and Table III indicate that the carbon and corresponding doped metal derived from MPcTa or M₂Pc₂Ha can efficiently enhance the conductivity of each composite. This electrochemical result corresponds to the speculation gained by the characterization of the SEM. Compared with mononuclear metal tetraaminophthalocyanines, MPcTa, binuclear metal hexaaminophthalocyanines, M₂Pc₂Ha, have larger molecular skeleton and flexibility, which is conducive to forming a small and homogeneous spherical particle and promoting the close packing of the materials. The uniform morphology is beneficial to the rapid diffusion of Li⁺ in the material, and the metal doping causes slight lattice distortions and defects, thereby improving the conductivity of the materials. The discharge capacity of pure LFP in practice is difficult to achieve the theoretical values of 170 mAh/g. This is due to the occurrence of oxygen evolution during the charging and discharging

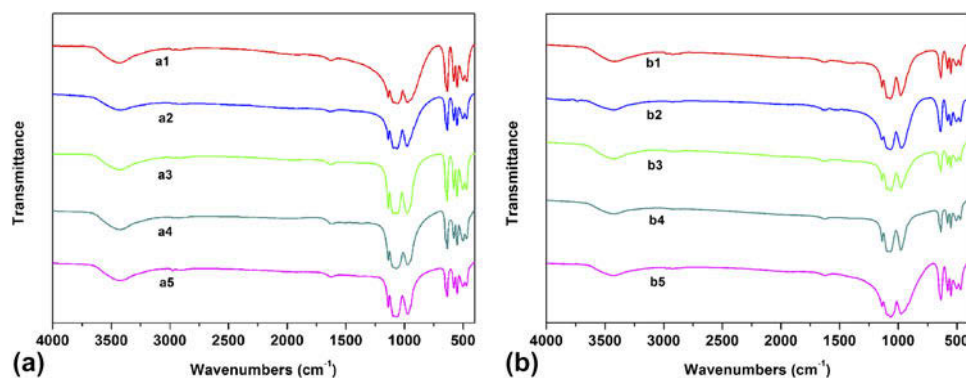


FIG. 2. IR spectra of (a) a1, a2, a3, a4, and a5 and (b) b1, b2, b3, b4, and b5.

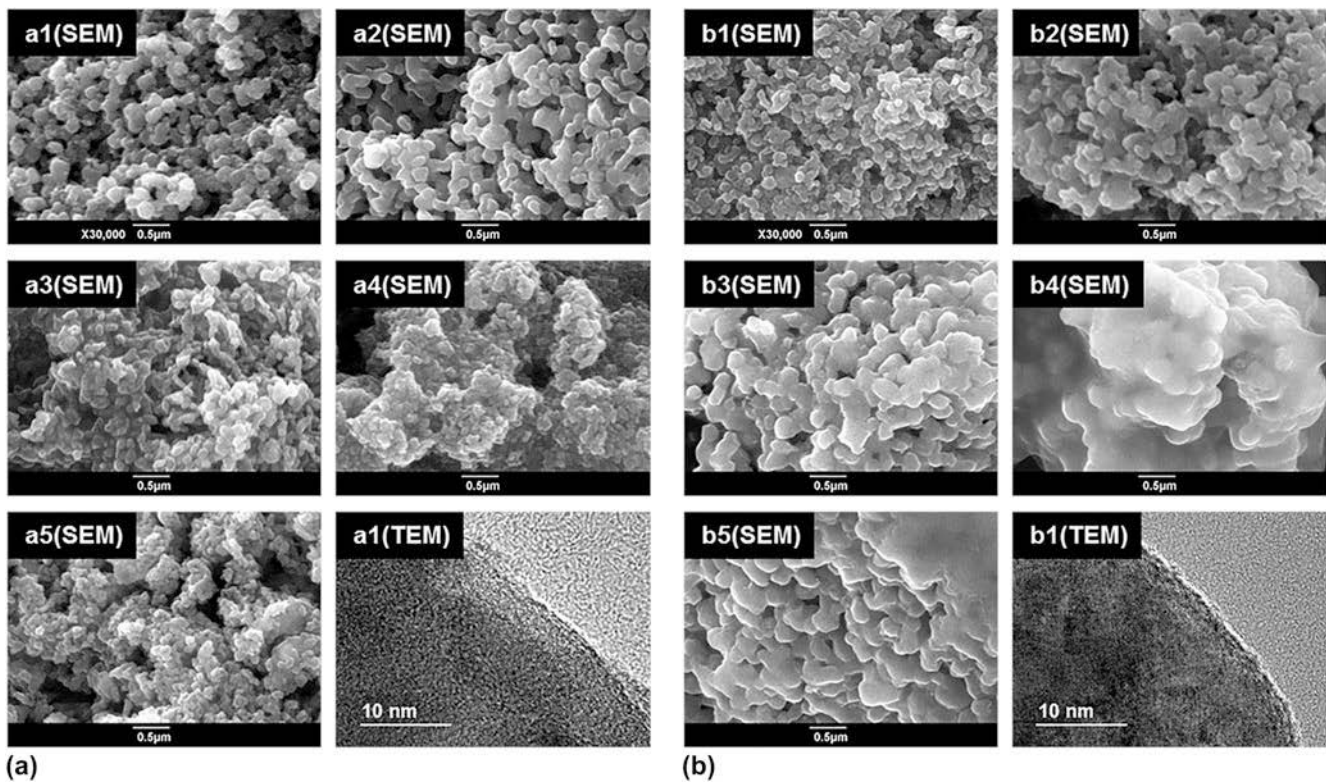


FIG. 3. SEM images of (a) a1, a2, a3, a4, a5, and high-resolution TEM of a1 and (b) b1, b2, b3, b4, b5, and high-resolution TEM of b1.

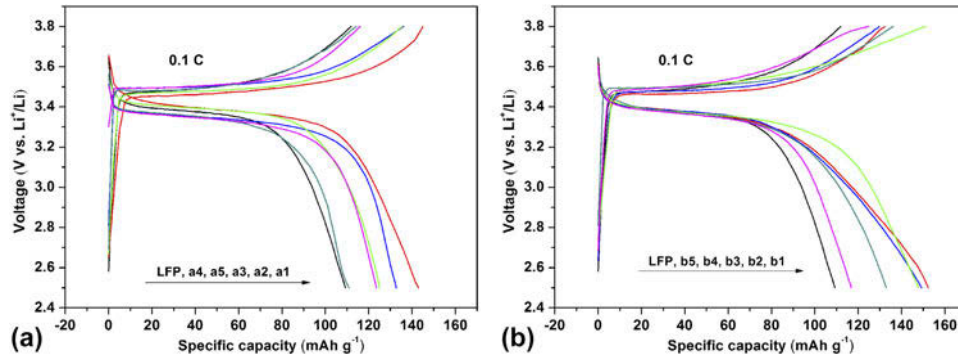


FIG. 4. Initial charge/discharge curves at 0.1 C of (a) a1, a2, a3, a4, a5, and pure LFP and (b) b1, b2, b3, b4, b5, and pure LFP.

TABLE III. Various parameters of the charge/discharge curves of the samples.

Sample	Charge specific capacity (mAh/g)	Charging medium voltage (V)	Discharge specific capacity (mAh/g)	Discharge medium voltage (V)	Coulombic efficiency (%)	Voltage difference (V)
a1	145.0	3.45	143.0	3.41	98.6	0.04
a2	136.2	3.50	132.7	3.36	97.4	0.14
a3	135.6	3.47	125.1	3.40	92.3	0.07
a4	114.3	3.48	110.9	3.37	97.0	0.11
a5	116.2	3.50	123.6	3.36	106.4	0.14
b1	132.4	3.46	152.3	3.38	115.0	0.08
b2	129.7	3.48	149.2	3.39	115.0	0.09
b3	151.1	3.50	147.7	3.39	97.7	0.11
b4	136.2	3.50	132.9	3.38	97.6	0.12
b5	124.9	3.49	116.8	3.38	93.5	0.11
LFP	111.9	3.50	109.2	3.39	97.6	0.11

process, which leads to the decrease of the electrochemical performance and the specific capacitance of the active materials. In addition, all the composites with relatively high coulombic efficiency (Table III) indicate a better Li⁺ reversible intercalation/deintercalation performance, which further proves that the composites own higher conductivity. Especially the coulombic efficiencies of a5, b1, and b2 are over 100%. In the testing process of the experiment, the charging process is first carried out and then the discharge is carried out. During the charging process, the cathode material is deintercalation lithium and the anode is intercalation lithium. In the half cell, the anode is Li, so the anode is sufficient for the lithium ion with respect to the cathode. And the charging process will consume a part of lithium to form the electrochemical impedance spectroscopy (SEI) film,^{29–31} which is a part of the loss of coulombic efficiency. In this paper, the coulombic efficiency of a5, b1, and b2 is higher than 100%; in addition to the above reasons, it may also be attributed to that Li⁺ ions occupy the Fe sites, which leads to that the initial discharge capacity is greater than the charge capacity.³²

To verify this conclusion, the electrochemical impedance spectroscopy (EIS) is further studied [Figs. 5(a) and 5(b)], which shows a well-defined semicircle in the high-frequency region followed by a linear part at a low-frequency region. The semicircle is related to the charge transfer process at the interface

between the electrode and the electrolyte, and the linear part corresponds to the Li⁺ diffusion behavior.^{33,34} To illustrate the electrochemical impedance spectrum, an equivalent circuit of the electrodes is present in Figs. 5(a) and 5(b) (inset). In the equivalent circuit, CPE represents the double layer capacitance, R_s stands for the resistance of the electrolyte and electrode, R_{ct} is on behalf of the resistance of the charge transfer, and W is the Warburg impedance. The charge transfer resistances in a1–a5 (125.8, 175.9, 252.7, 351.9, 296.7 Ω) or b1–b5 (58.7, 94.6, 105.9, 166.5, 350.0 Ω) are all significantly lower than the pure LFP (401.7 Ω). On the whole, the charge transfer resistance of b-series is smaller than a-series. The EIS results are consistent with the facts of charge/discharge assays. For further investigation, the lithium-ion diffusion coefficient is calculated according to the low frequency region of EIS by using equation (1)^{35–37}:

$$D = \frac{R^2 T^2}{2A^2 n^4 F^4 c^2 \sigma_w^2} , \quad (1)$$

where R and T are the gas constant [8.3144621 J/(mol K)] and the absolute temperature, A is on behalf of the surface areas of the electrode, n and F represent the number of transfers per molecule and Faraday constant (96,485 C/mol), and c and σ_w stand for the concentration of lithium and Warburg coefficient. In addition, the

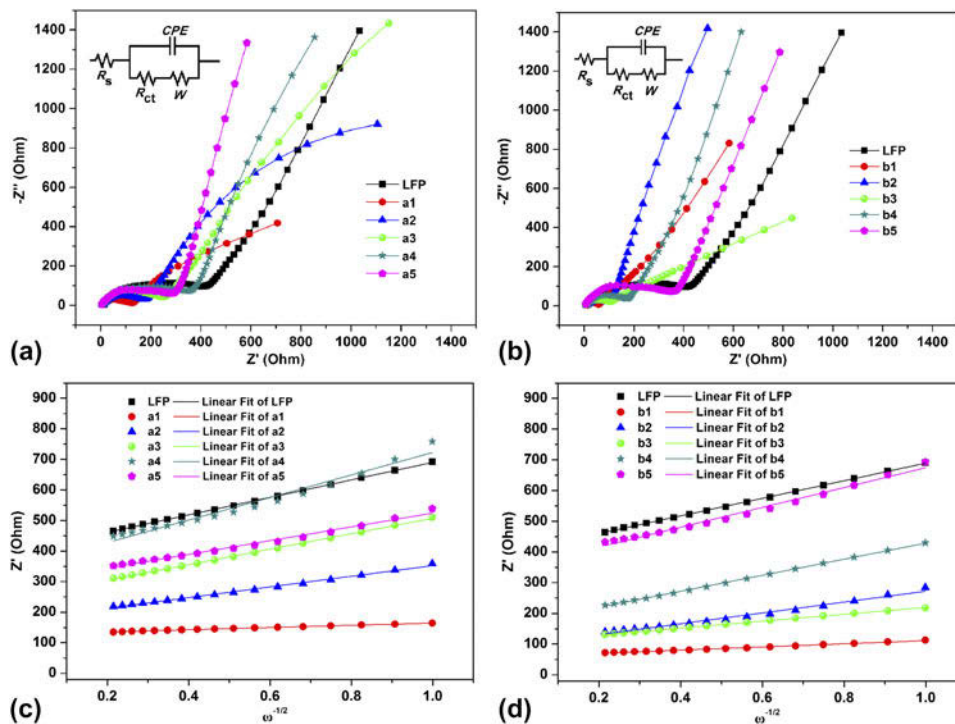


FIG. 5. EIS spectra of samples (a) a1–a5 and (b) b1–b5, and fitting plots between Z' and $\omega^{-1/2}$ in the low-frequency region of samples (c) a1–a5 and (d) b1–b5.

diffusion coefficient of lithium ion is inversely proportional to the Warburg coefficient σ_w as follows:

$$Z' = R_s + R_{ct} + \sigma_w \omega^{-1/2} , \quad (2)$$

where ω is the angular frequency. The Warburg factor σ_w can be calculated by the linear fitting of Z' and the reciprocal square root of the angular frequency (ω), as shown in Figs. 5(c) and 5(d), and the data are given in Table IV. It is noteworthy that the diffusion coefficient of a1 and b1 is more excellent and their charge transfer resistances are dramatic.

The above characterization and electrical performance test results demonstrate that the capacity performance of a1 and b1 is better in the same series. To further research the effect of different additives on the electrochemical performance of the composite materials, the cyclic voltammogram (CV) profiles of a1, b1, and pure LFP are shown in Fig. 6. The test method is linear scan cyclic voltammetry, and the voltage range is controlled between 2 and 4.2 V, the scan rate is 0.001 V/s, and the sampling interval is 0.001 V. As seen from the CV curves, the oxidation peaks and reduction peaks of the three samples are highly symmetric, and the peaks of a1 and b1 exhibit higher symmetry compared with pure LFP, which

TABLE IV. Resistances derived from EIS based on the proposed circuit model and the diffusion coefficients of Li⁺ for samples a1–a5 and b1–b5.

Sample	R_s (Ω)	R_{ct} (Ω)	σ_w (Ω cm ² /s ^{1/2})	D (cm ² /s)
a1	2.1	125.8	36.53	6.48×10^{-11}
a2	2.1	175.9	174.52	2.84×10^{-12}
a3	2.1	252.7	252.18	1.36×10^{-12}
a4	2.2	351.9	368.72	6.36×10^{-13}
a5	2.3	296.7	225.51	1.70×10^{-12}
b1	2.2	58.7	51.60	3.25×10^{-11}
b2	2.1	94.6	176.58	2.77×10^{-12}
b3	2.1	105.9	112.60	6.82×10^{-12}
b4	2.0	166.5	261.01	1.27×10^{-12}
b5	2.3	350.0	323.00	8.29×10^{-13}
LFP	2.3	401.7	286.15	1.06×10^{-12}

manifests that the materials of a1 and b1 have better reversibility. The high peak intensity and small potential difference are indications of the good reversibility of Li⁺ intercalation/deintercalation reactions and excellent kinetics.^{38,39} The potential difference of pure LFP is 0.83 V, whereas those of a1 and b1 are 0.77 V and 0.97 V, respectively. From an overall perspective, the CV curves of a1 and b1 have better symmetry than pure LFP, suggesting that the samples have higher electrochemical activity and better crystallinity,⁴⁰ which reflects the decreased polarization and the increased diffusion rate of lithium ion. In addition, lithium ions and electrons in the system of a1 and b1 are more active, depending on homogenous morphology (SEM) of nanoparticles composites, which can shorten the Li⁺ diffusion pathway and improve the reversibility of Li⁺ intercalation/deintercalation process.

To research the rate capability, the materials a1, b1, and pure LFP were recorded by galvanostatic cycling at various charge–discharge currents from 0.1 C to 5 C each for 10 cycles (Fig. 7). In all cases, the specific capacity decreases with the current density increasing, which manifests low active material utilization and transport limitations in the electrode materials. At a very low current rate of 0.1 C, the discharge specific capacity of a1 (143.0 mAh/g) is slightly lower than b1 (152.3 mAh/g) and significantly larger than pure LFP (109.2 mAh/g). Nevertheless, the discharge specific capacities of pure LFP is 68.5 mAh/g after 60 cycles at 5 C, which decreases notably compared with 0.1 C, showing the capacity retention of 37.3%. However, under the same conditions, the capacity retention of a1 (68.5%) and b1 (90.4%) is remarkably higher than pure LFP. The discharge specific capacities of LiFePO₄ modified by binuclear metal hexaaminophthalocyanines are higher than that of mononuclear metal tetraaminophthalocyanines, since the larger molecular skeleton possesses a relatively good conjugation and is more effective modification of LFP. And the radius of the manganese ion approaches that of the iron ion, so it is easy to enter the lattice of LFP. Manganese makes the LFP more stable and further improves the electrochemical performance of LFP for

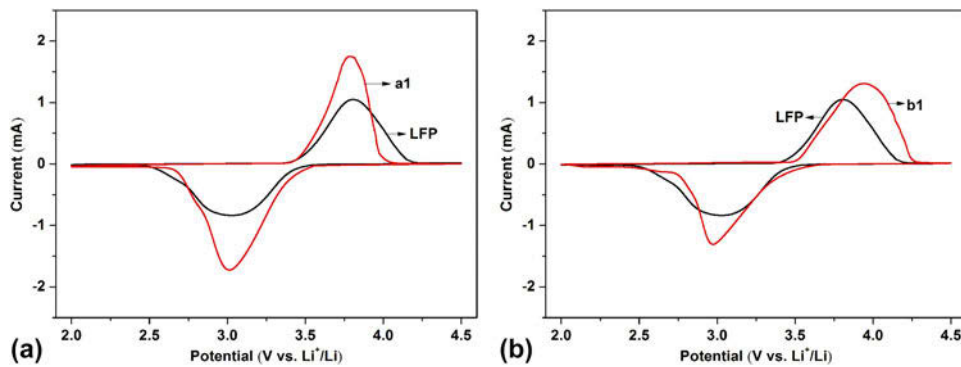


FIG. 6. CV curves of samples (a) a1 and (b) b1 at 0.1 mV/s.

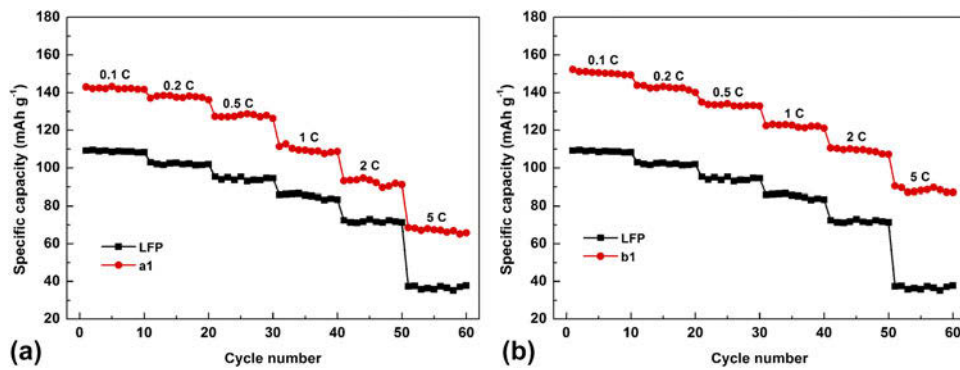


FIG. 7. Rate performance of samples (a) a1 and (b) b1.

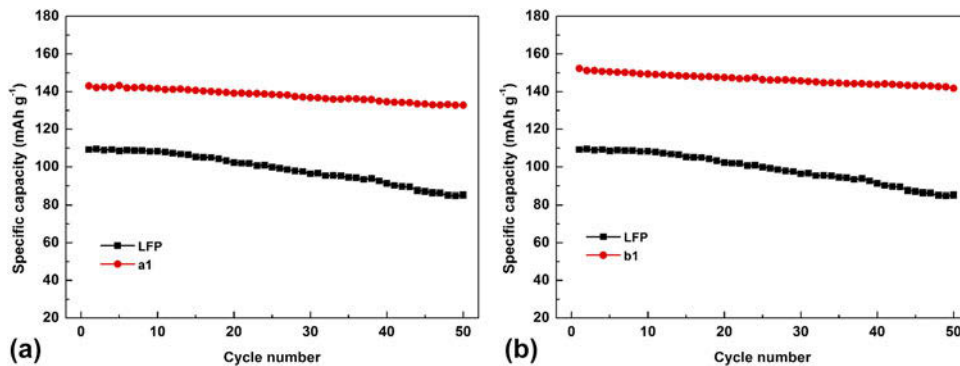


FIG. 8. Cycling performance of samples (a) a1 and (b) b1 at 0.1 C.

a LIB.⁴¹ The cycle performance of three samples at 0.1 C is showed in Fig. 8. After 50 cycles, the capacity retention of a1 is 92.8%, which is much better than that of the pure LFP (87.2%) but slightly lower than that of b1 (93.0%). It is showed that MnPcTa or Mn₂Pc₂Ha as additives to modify the LFP can excellently improve the cycle life of the batteries.

IV. CONCLUSIONS

In summary, MPcTa or M₂Pc₂Ha is used as additives to synthesize LiFe_{1-x}M_xPO₄/C [$x \approx 0.0040$; M = Mn(II), Co(II), Ni(II), Cu(II), Zn(II)]. The carbon layer is uniformly coated on the surface of the composites, which provides a fast channel for electron transfer in the process of charging and discharging. Moreover, the doping of metals can cause a certain extent lattice defects of LFP and improve the conductivity of the composites. This research shows that binuclear metal hexaaminophthalocyanines as additives display more excellent electrochemical performances. In particular, the compound of binuclear manganese hexaaminophthalocyanines as an additive can achieve the highest initial discharge specific capacity of 152.3 mAh/g at 0.1, and the low charge transfer resistance is 58.7 Ω. Combined with the above characteristics, the composite materials have remarkable conductivity, electrochemical

reversibility, and high stability, so they can be better used in the field of electronics.

ACKNOWLEDGMENTS

The authors thank the National Natural Science Foundation of China (Nos. 21401149 and 21371143) and Natural Science Foundation of Shaanxi Province (No. 2015JM2062) for the financial support of this work.

REFERENCES

1. J.B. Goodenough and Y. Kim: Challenges for rechargeable Li batteries. *Chem. Mater.* **22**, 587 (2009).
2. J.B. Goodenough and K.S. Park: The Li-ion rechargeable battery: A perspective. *J. Am. Chem. Soc.* **135**, 1167 (2013).
3. M.K. Devaraju and I. Honma: Hydrothermal and solvothermal process towards development of LiMPO₄ (M = Fe, Mn) nano-materials for lithium-ion batteries. *Adv. Energy Mater.* **2**, 284 (2012).
4. Q. Fan, L. Lei, and X. Xu: Direct growth of FePO₄/graphene and LiFePO₄/graphene hybrids for high rate Li-ion batteries. *J. Power Sources* **257**, 65 (2013).
5. B.L. Ellis, K.T. Lee, and L.F. Nazar: Positive electrode materials for Li-ion and Li-batteries. *Chem. Mater.* **22**, 691 (2010).
6. T.F. Liu, L. Zhao, J.S. Zhu, B. Wang, C.F. Guo, and D.L. Wang: Challenges for rechargeable Li batteries. *Chem. Mater.* **2**, 2822 (2014).

7. J. Wang and X. Sun: Understanding and recent development of carbon coating on LiFePO₄ cathode materials for lithium-ion batteries. *Energy Environ. Sci.* **5**, 5163 (2012).
8. H. Zhang, Y. Xu, C. Zhao, X. Yang, and Q. Jiang: Effects of carbon coating and metal ions doping on low temperature electrochemical properties of LiFePO₄ cathode material. *Electrochim. Acta* **83**, 341 (2012).
9. L.X. Li, X.C. Tang, H.T. Liu, Y. Qu, and Z.G. Lu: Morphological solution for enhancement of electrochemical kinetic performance of LiFePO₄. *Electrochim. Acta* **56**, 995 (2010).
10. A. Yamada, S.C. Chung, and K. Hinokuma: Optimized LiFePO₄ for lithium battery cathodes. *J. Electrochem. Soc.* **148**, A224 (2001).
11. Y. Xia, W.K. Zhang, H. Huang, Y.P. Gan, J. Tian, and X.Y. Tao: Self-assembled mesoporous LiFePO₄ with hierarchical spindle-like architectures for high-performance lithium-ion batteries. *J. Power Sources* **196**, 5651 (2011).
12. S. Praneetha and A. Vadivel Murugan: A rapid, one-pot microwave-solvothermal synthesis of a hierarchical nanostructured graphene/LiFePO₄ hybrid as a high performance cathode for lithium ion batteries. *RSC Adv.* **3**, 25403 (2013).
13. B. Wang, B. Xu, T. Liu, P. Liu, C. Guo, S. Wang, Q. Wang, Z. Xiong, D. Wang, and X.S. Zhao: Mesoporous carbon-coated LiFePO₄ nanocrystals co-modified with graphene and Mg²⁺ doping as superior cathode materials for lithium ion batteries. *Nanoscale* **6**, 986 (2014).
14. R. Wang, R. Zhang, B. Xu, F. Yang, and J. Zhao: Highly improving the electrochemical performance of LiFePO₄ modified by metal phthalocyanines as cathode materials. *J. Mater. Res.* **30**, 645 (2015).
15. R.Q. Wang, R.L. Zhang, B. Xu, F. Yang, J.S. Zhao, S.C. Zhang, and J.L. Wang: Metal tetrabromophthalocyanines mediate the structure and electrochemical performance of lithium iron phosphate as cathode materials for lithium-ion batteries. *J. Electroanal. Chem.* **755**, 47 (2015).
16. G. Ramos-Sánchez, A. Callejas-Tovar, L.G. Scanlon, and P.B. Balbuena: DFT analysis of Li intercalation mechanisms in the Fe-phthalocyanine cathode of Li-ion batteries. *Phys. Chem. Chem. Phys.* **16**, 743 (2014).
17. R.L. Zhang, R.Q. Wang, and K. Luo: Multi-walled carbon nanotubes chemically modified by cobalt tetraaminophthalocyanines with excellent electrocatalytic activity to Li/SOCl₂ battery. *J. Electrochem. Soc.* **161**, H941 (2014).
18. B. Xu, R.L. Zhang, J.F. Wang, and J.S. Zhao: Investigation of binuclear metal phthalocyanines as electrocatalysts for Li/SOCl₂ battery. *J. Solid State Electrochem.* **17**, 2391 (2013).
19. R. Wang, R. Zhang, B. Xu, F. Yang, and J. Zhao: Highly improving the electrochemical performance of LiFePO₄ modified by metal phthalocyanines as cathode materials. *J. Mater. Res.* **30**, 645 (2015).
20. Y. Qiao, L. Pan, and P. Jia: Effect of magnetic treatment on microstructure and cycle performance of LiFePO₄/C cathode material. *Mater. Lett.* **137**, 432 (2014).
21. X. Hairong, Z. Jianqing, W. Tao, G. Hu, F. Xiaoli, and H. Jianping: Facile and economical synthesis for “plum pudding”-shaped porous LiFePO₄/carbon composites for lithium ion batteries. *RSC Adv.* **4**, 39400 (2014).
22. Y. Xie, F. Song, C. Xia, and H. Du: Preparation of carbon-coated lithium iron phosphate/titanium nitride for a lithium-ion supercapacitor. *New J. Chem.* **39**, 604 (2015).
23. L. Wang, X. He, and W. Sun: Crystal orientation tuning of LiFePO₄ nanoplates for high rate lithium battery cathode materials. *Nano Lett.* **12**, 5632 (2012).
24. L.F. Di, G. Meligrana, C. Gerbaldi, S. Bodoardo, and N. Penazzi: Surfactant-assisted mild solvothermal synthesis of nanostructured LiFePO₄/C cathodes evidencing ultrafast rate capability. *Electrochim. Acta* **156**, 188 (2015).
25. X. Xu, Y. Xu, H. Zhang, M. Ji, and H. Dong: The effect of NiO as graphitization catalyst on the structure and electrochemical performance of LiFePO₄/C cathode materials. *Electrochim. Acta* **158**, 348 (2015).
26. A. Örnek and O. Efe: Doping qualifications of LiFe_{1-x}Mg_xPO₄-C nano-scale composite cathode materials. *Electrochim. Acta* **166**, 338 (2015).
27. N. Bai, H. Chen, W. Zhou, K. Xiang, Y. Zhang, C. Li, and H. Lu: Preparation and electrochemical performance of LiFePO₄/C microspheres by a facile and novel co-precipitation. *Electrochim. Acta* **167**, 172 (2015).
28. A. Yamada, S.C. Chung, and K. Hinokuma: Optimized LiFePO₄ for lithium battery cathodes. *J. Electrochem. Soc.* **148**, A224 (2001).
29. D. Aurbach, E. Zinigrad, Y. Cohen, and H. Teller: A short review of failure mechanisms of lithium metal and lithiated graphite anodes in liquid electrolyte solutions. *Solid State Ionics* **148**, 405 (2002).
30. D. Ostrovskii, F. Ronci, B. Scrosati, and P. Jacobsson: A FTIR and Raman study of spontaneous reactions occurring at the LiNi_yCo_(1-y)O₂ electrode/non-aqueous electrolyte interface. *J. Power Sources* **94**, 183 (2001).
31. K.A. Striebel, E. Sakai, and E.J. Cairns: Impedance studies of the thin film LiMn₂O₄/electrolyte interface. *J. Electrochem. Soc.* **149**, A61 (2002).
32. L. Wang, W. Sun, and X. Tang: Nano particle LiFePO₄ prepared by solvothermal process. *J. Power Sources* **244**, 94 (2013).
33. J.Y. Xiang, J.P. Tu, and L. Zhang: Improved electrochemical performances of 9LiFePO₄·Li₃V₂(PO₄)₃/C composite prepared by a simple solid-state method. *J. Power Sources* **195**, 8331 (2010).
34. T. Muraliganth, A.V. Murugan, and A. Manthiram: Nanoscale networking of LiFePO₄ nanorods synthesized by a microwave-solvothermal route with carbon nanotubes for lithium ion batteries. *J. Mater. Chem.* **18**, 5661 (2008).
35. H. Shu, X. Wang, and Q. Wu: Improved electrochemical performance of LiFePO₄/C cathode via Ni and Mn co-doping for lithium-ion batteries. *J. Power Sources* **237**, 149 (2013).
36. X. Wang, H. Hao, J. Liu, T. Huang, and A. Yu: A novel method for preparation of macroporous lithium nickel manganese oxygen as cathode material for lithium ion batteries. *Electrochim. Acta* **56**, 4065 (2011).
37. X.Y. Wang, Q. Cheng, T. Huang, and A.S. Tao: Effect of calcination atmosphere on Li/Ni disorder and electrochemical performance of layered LiNi_{0.5}Mn_{0.5}O₂. *Acta Phys.-Chim. Sin.* **27**, 437 (2011).
38. H. Liu, C. Li, and H.P. Zhang: Kinetic study on LiFePO₄/C nanocomposites synthesized by solid state technique. *J. Power Sources* **159**, 717 (2006).
39. L. Ji, Y. Yao, and O. Toprakci: Fabrication of carbon nanofiber-driven electrodes from electrospun polyacrylonitrile/polypyrrole bicomponents for high-performance rechargeable lithium-ion batteries. *J. Power Sources* **195**, 2050 (2010).
40. C. Delacourt, C. Wurm, and L. Laffont: Electrochemical and electrical properties of Nb- and/or C. *Solid State Ionics* **177**, 333 (2006).
41. M.B. Sahana, S. Vasu, N. Sasikala, S. Anandan, H. Sepehri-Amin, C. Sudakar, and R. Gopalan: Raman spectral signature of Mn-rich nanoscale phase segregations in carbon free LiFe_{1-x}Mn_xPO₄ prepared by hydrothermal technique. *RSC Adv.* **4**, 64429 (2014).